crystals

MDPI

Review

The Effect of Ligand Design on Metal Ion Spin State—Lessons from Spin Crossover Complexes

Malcolm A. Halcrow

School of Chemistry, University of Leeds, Woodhouse Lane, Leeds LS2 9JT, UK; m.a.halcrow@leeds.ac.uk; Tel.: +44-113-343-6506

Academic Editor: Martin T. Lemaire
Received: 22 April 2016; Accepted: 13 May 2016; Published: 18 May 2016

Abstract: The relationship between chemical structure and spin state in a transition metal complex has an important bearing on mechanistic bioinorganic chemistry, catalysis by base metals, and the design of spin crossover materials. The latter provide an ideal testbed for this question, since small changes in spin state energetics can be easily detected from shifts in the spin crossover equilibrium temperature. Published structure-function relationships relating ligand design and spin state from the spin crossover literature give varied results. A sterically crowded ligand sphere favors the expanded metal–ligand bonds associated with the high-spin state. However, steric clashes at the molecular periphery can stabilize either the high-spin or the low-spin state in a predictable way, depending on their effect on ligand conformation. In the absence of steric influences, the picture is less clear since electron-withdrawing ligand substituents are reported to favor the low-spin or the high-spin state in different series of compounds. A recent study has shed light on this conundrum, showing that the electronic influence of a substituent on a coordinated metal ion depends on its position on the ligand framework. Finally, hydrogen bonding to complexes containing peripheral N–H groups consistently stabilizes the low-spin state, where this has been quantified.

Keywords: transition metals; spin state; spin crossover; structure–function relationships; magnetostructural correlations; magnetic measurements

1. Introduction

In principle, controlling the spin state of a coordinated transition ion through ligand design should be a straightforward problem of coordination chemistry. Undergraduate crystal field theory teaches that octahedral metal ions with d^4–d^7 electron counts can adopt either a high-spin or a low-spin configuration, corresponding to the maximum or minimum possible number of unpaired electrons (Scheme 1) [1]. Whether a compound is high- or low-spin depends on a competition between the crystal field orbital splitting (Δ_{oct}) and the intra-orbital electron pairing energy (P), which are both unfavorable energy terms. If $\Delta_{oct} < P$ it is less costly to populate the e_g orbital subshell than to pair electrons in the t_{2g} orbitals, leading to the adoption of a high-spin state. If $\Delta_{oct} > P$ the converse is true, and a low-spin state is favored (Scheme 1). The magnitude of P is effectively constant for a particular metal ion in a given coordination geometry, being a function of its electron configuration and effective nuclear charge. Hence, all other things being equal, the spin state of a complex is controlled by the strength of the ligand field around the metal ion, as defined by Δ_{oct}. The same arguments can be generalized to other coordination geometries, although the d-electron counts that can show a high-spin/low-spin dichotomy vary according to the relevant d-orbital splitting. Among other things, a large Δ and a low-spin state are favored by ligands near the top of the spectrochemical series, most of which have π-acceptor capability; by a tetragonal coordination geometry, which strongly differentiates the on-axis (d_{x2-y2}/d_{z2}) and off-axis ($d_{xy}/d_{xz}/d_{yz}$) d-orbitals; and by heavier second and third row metals, with more diffuse valence d-orbitals and stronger metal–ligand covalency.

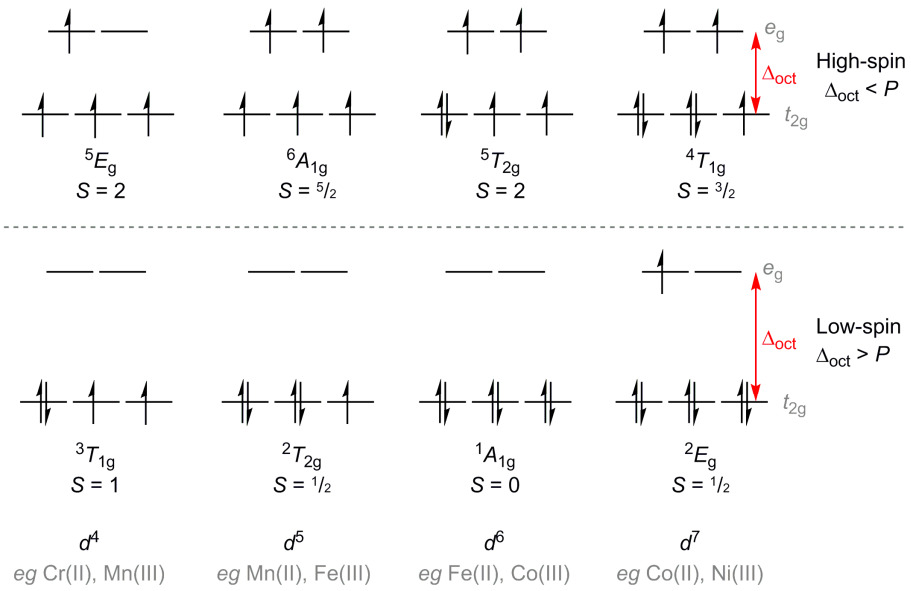

Scheme 1. High-spin and low-spin electron configurations of d^4–d^7 transition ions in an octahedral ligand field, with their weak-field term symbols and spin quantum numbers [2].

This apparently simple question has an important bearing on a number of areas of transition metal reactivity [3]. Most simply, the spin state of a metal ion determines its reactivity towards ligand substitution. The high-spin state of a metal ion always contains more electrons in metal-ligand antibonding *d*-orbitals (the e_g subshell in Scheme 1), leading to weaker M–L bonds and a lower crystal field activation energy than the low-spin state. Thus, high-spin complexes are generally more kinetically labile. Obtaining quantitative data comparing substitution rates of the same metal center in two spin states is a challenging problem [4]. However, a qualitative example is provided by $[Fe(3\text{-bpp})_2]^{2+}$ (Scheme 2), which has a 70% ± 10% low-spin population in aqueous solution at room temperature and is stable in water for a period of days [5,6]. This contrasts with its isomer $[Fe(1\text{-bpp})_2]^{2+}$ (Scheme 2), which is 90% high-spin in solution at room temperature and hydrolyzes spontaneously in contact with water [5]. The difference probably arises from strong N–H···OH_2 hydrogen bonding undertaken by $[Fe(3\text{-bpp})_2]^{2+}$ in aqueous solution, which makes the 3-bpp ligands more electron rich by increasing the $N^{\delta-}$–$H^{\delta+}$ bond polarity (see below). More subtly, the involvement of high-spin intermediates in substitution reactions of low-spin complexes can lead to a change in mechanism and increase in reaction rate [3,7].

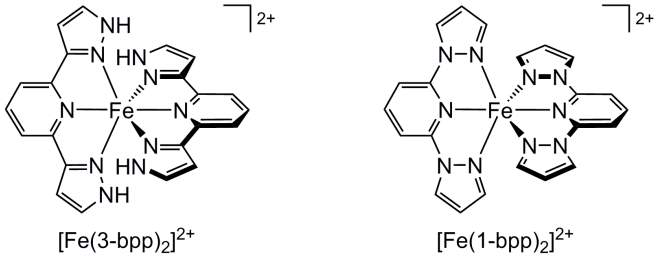

Scheme 2. The structures of $[Fe(3\text{-bpp})_2]^{2+}$, which is stable in aqueous solution, and $[Fe(1\text{-bpp})_2]^{2+}$, which is not.

Another generalization is that high-spin complexes, with their increased radical character, are more prone towards single-electron reactivity than low-spin metal centers. This is particularly relevant in biological and synthetic oxidation catalysis, which most commonly involves high-valent iron or manganese intermediates whose spin states are malleable, depending on the co-ligands present.

The two-step radical rebound mechanism typically adopted by these reactions involves an initial, rate-limiting H• atom abstraction from the substrate. That is favored by free-radical catalyst oxidant species, which generate unpaired spin density on the reactive oxo ligand centers [3,8]. The Fe=O (ferryl) intermediates in heme enzymes get round this problem particularly elegantly, by combining a low-spin Fe(IV) ion (for kinetic stability) with a porphyrin cation ligand radical to initiate the radical rebound [9]. Many non-heme enzymes and synthetic complexes adopt the alternative approach of using weak field ligands to generate a high-spin ferryl active oxidant [10]. Comparisons of synthetic iron(IV) ferryl species with $S = 1$ and $S = 2$ ground states have shown that the latter are consistently more reactive towards H• atom abstraction from a substrate [4,11].

Such considerations can also have a bearing on organometallic catalysis, where first-row transition ions are increasingly playing a role [12]. An important example is provided by the complexes in Scheme 3, which are highly active pre-catalysts for the polymerization of styrene [13]. Activation of the complexes with (2-chloroethyl)benzene affords five-coordinate iron(III) active catalysts [LFeCl$_2$(C$_2$H$_4$Ph)], where L is the α-diimine chelate. Interestingly, the active intermediates formed from **A** have a high-spin state ($S = {}^5/_2$), which undergo atom transfer radical polymerization (ATRP) with all the characteristics of a living polymerization reaction. In contrast, the five-coordinate activated species formed from **B** have a reduced, intermediate spin state ($S = {}^3/_2$). This strongly disfavors atom transfer chemistry, leading to a much slower catalytic chain transfer process yielding low molecular-weight polymer product [13]. The difference is caused by the inductive effect of the ligand phenyl substituents in **B**, which promote iron→diimine back bonding sufficiently to induce a spin state flip [14].

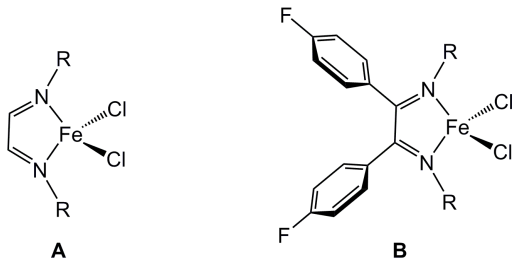

Scheme 3. Structures of alkene polymerization pre-catalysts that proceed by rapid atom radical transfer polymerization (**A**) or a slow chain transfer reaction (**B**; R = cyclohexyl or *tert*butyl) [13].

A final, rather different consequence of the existence of high- and low-spin states in metal complexes is spin crossover (SCO); that is, a transition between spin states in a molecule or material under the action of a physical stimulus [15–17]. This is most often observed upon heating or cooling the sample, but spin state changes can also be produced under high pressure (*ca*. 1 GPa), by a strong magnetic field, or, in the solid state, by irradiating the sample. Where individual switching centers (molecules) are isolated from each other or are otherwise weakly interacting, as in solution for example, thermal SCO is observed as a gradual Boltzmann-type equilibrium [15,18]. More efficient packing of switching centers in molecular solids or coordination polymers can lead to more cooperative SCO switching, occurring abruptly and/or with thermal hysteresis (which leads to genuine spin state bistability) [19]. Such compounds have added interest because of the changes in their physical properties that accompany SCO [20]. Most obvious is the expected change in magnetic moment, which leads to diamagnetic/paramagnetic switching in iron(II) complexes for example (Scheme 1). However, SCO in different compounds also leads to changes in color; fluorescence; conductivity (in the bulk or at the single molecule level); and/or dielectric constant [15]. It can also lead to a measurable mechanical response in a solid sample [21]. SCO materials can be fabricated at the nanoscale, retaining their switching functionality at least partially in the 10^1–10^2 nm size regime [22]. This combination of versatility, multifunctionality, and fabricability has made SCO compounds one of the most popular forms of molecular switch in molecular materials research.

Tuning spin state properties for catalysis or for switchable materials requires an understanding of how the spin state of a complex is influenced by its molecular structure. While it is well understood how factors such as metal oxidation state and coordination geometry control Δ_{oct} and spin state (see above), the influence of ligand design on spin state is more subtle and harder to predict. Spin crossover complexes are particularly suited to this question, because small changes in spin state energetics between different compounds are measurable, in principle, via the SCO equilibrium midpoint temperature ($T_{½}$). For example, a 10 K shift in $T_{½}$ corresponds to a change of *ca.* 1 kJmol^{-1} in the relative enthalpies of the spin states or *ca.* 5 Jmol^{-1}K^{-1} in their relative entropies, all other things being equal. While SCO is usually measured in the solid state, such small changes are better studied in solution, where molecules undergo SCO independently of their neighbors [15,18]. That allows their molecular properties to be measured without contamination from lattice effects, which can have a large influence on SCO in solid samples [19]. While the influence of ligand displacement reactions and secondary bonding interactions with a solvent must be guarded against, these are easily detected when measuring SCO in solution [23].

This article surveys the SCO literature to determine how the spin state of a complex is influenced by the nature of its ligands. Solution phase measurements are emphasized, for the reasons in the previous paragraph, but solid state data are also presented where they add to the discussion and are clearly distinguished in the text.

2. Results

2.1. Steric Influence of Ligand Substituents on Metal Ion Spin States

As mentioned previously, high-spin complexes always have more electrons in e_g-type *d*-orbitals, which are metal–ligand antibonding, than the corresponding low-spin forms (Scheme 1). Hence, high-spin complexes would be expected to have longer, and weaker, M–L bonds. In practice this difference is more pronounced for some metal–ligand combinations than for others. For example, SCO in d^5 or d^6 metal ions like iron(III) or iron(II), which involves a $\Delta S = \pm 2$ spin state change, has a greater effect on their molecular structure than the $\Delta S = \pm 1$ SCO undergone by d^4 and d^7 centers [manganese(III) or cobalt(II)]. The strong Jahn–Teller elongation distortions exhibited by the high-spin d^4 and low-spin d^7 configurations also affect the structural changes during SCO in complexes of those ions. Moreover, bonds to harder N, O-donor ligands tend to be more sensitive to metal ion spin state than softer P, S or halide ligand donors [24]. However, in iron(II) SCO complexes with N-donor ligands, for example, the Fe–L bonds can be up to 10% longer in the high-spin state than the low-spin. Hence, one would expect a sterically crowded ligand sphere to consistently favor the high-spin state of a complex.

There are a number of SCO systems that bear out that assumption. The first clear demonstration was with the [Fe(Py$_3$tren)]$^{2+}$ podand complex system (Figure 1). The parent complex [Fe(Py$_3$tren)]$^{2+}$ is low-spin at room temperature, but methylation of the pyridyl *C*6 positions (which are in close proximity to the iron atom) induces SCO behavior. Notably, the temperature of SCO decreases with an increased number of methyl groups in [Fe(Me$_x$Py$_3$tren)][PF$_6$]$_2$, following the trend $x = 1$ ($T_{½} \approx 433$ K) > $x = 2$ (290 K) > $x = 3$ (219 K) in the solid state, and $x = 1$ ($T_{½} \approx 430$ K) > $x = 2$ (319 K) >> $x = 3$ (high-spin) in solution [25]. That is, sequential methylation of the complex consistently stabilizes the high-spin state of the complex. Comparison of their crystal structures clearly shows the steric crowding between the methyl group of one arm of the podand and the pyridyl group of its neighbor, which inhibits contraction of the Fe–N bonds associated with the transition to a low-spin state (Figure 1). These results have been used more recently to produce SCO metallomesogens based on an [Fe(Me$_x$Py$_3$tren)]$^{2+}$ core [26].

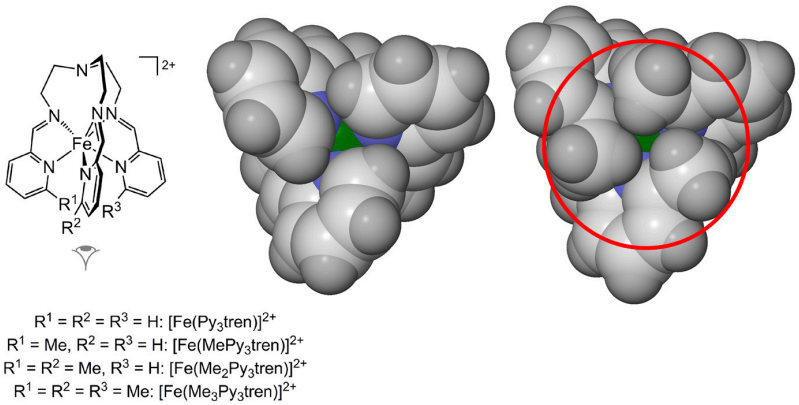

Figure 1. $[Fe(Py_3tren)]^{2+}$ and its methylated derivatives (**left**); and crystallographic space-filling views of $[Fe(Py_3tren)]^{2+}$ (center) and $[Fe(Me_3Py_3tren)]^{2+}$ (**right**) highlighting the steric influence of the methyl substituents in the latter compound [27,28]. The orientation of the space-filling views is indicated in the structure diagram. Color code: C, white; H, pale gray; Fe, green; N, blue.

Other studies that have drawn similar conclusions, based on solution measurements, involve the compounds shown in Scheme 4. The SCO equilibrium for $[Co(R_2impy)_2]^{2+}$ in $(CD_3)_2CO$ shifts to lower temperature according to the trend R = Bn > *i*Pr ≈ Tol > *t*Bu (the *tert*butyl complex remains high-spin at all temperatures) [29]. The low-spin complex $[Fe(bipy)_3]^{2+}$ becomes fully high-spin when methylated at the pyridyl *C*6 positions, as in $[Fe(mbpy)_3]^{2+}$ [30] and $[Fe(dmbpy)_3]^{2+}$ [31]. A series of iron(II) complexes based on tetradentate *tris*-(pyrid-2-ylmethyl)amine (tpa), $[Fe(tpa)(NCMe)_2]^{2+}$, also shows steadily increasing stabilization of the high-spin state as the tpa pyridyl *C*6 atoms are sequentially methylated [32]. The SCO equilibrium temperatures in the scorpionate complexes $[Fe(HB\{pz\}_y\{dmpz\}_{3-y})_2]$ shift progressively to higher temperature as the number of methyl groups in the complex increases, with fully substituted $[Fe(HB\{dmpz\}_3)_2]$ being high-spin [33–35]. The hexadentate ligand complex $[Fe(tpen)][ClO_4]_2$ is SCO-active in solution ($T_{½}$ = 363 K in dmf), while its dimethylated analogue $[Fe(btpen)][ClO_4]_2$ remains high-spin at all temperatures [36].

The unsubstituted macrocyclic complex $[Fe(Pytacn)(NCMe)_2]^{2+}$ is predominantly low-spin at room temperature in CD_3CN, but three analogues $[Fe(Py^{6-R}tacn)(NCMe)_2]^{2+}$ bearing substituents at the pyridyl *C*6 position are all high-spin under the same conditions [37]. Unsubstituted $[Fe(1\text{-}bpp)_2]^{2+}$ (Scheme 2) is SCO-active, with $T_{½}$ = 248 K in $(CD_3)_2CO$ [38], but $[Fe(R_2\text{-}1\text{-}bpp)_2]^{2+}$ are fully high-spin in the same solvent when R = Ph or *i*Pr [39]. The same trend is shown by the isomeric 3-bpp complex series, in that $[Fe(3\text{-}bpp)_2]^{2+}$ itself (Scheme 2) is SCO-active [5] but four $[Fe(R_2\text{-}3\text{-}bpp)_2]^{2+}$ derivatives with R ≠ H are all fully high-spin [40]. Like most derivatives of $[Fe(terpy)_2]^{2+}$, $[Fe(terpy)_2]^{2+}$ itself is low-spin when R = H, but $[Fe(Ph_2terpy)_2]^{2+}$ undergoes SCO ($T_{½}$ ≈ 300 K in EtCN solution) [41].

Finally, a similar conclusion was reached for a rather different series of compounds, namely tetrahedral $[(PhB\{MesIm\}_3)FeN{=}PR_3]$. A linear relationship between $T_{½}$ and the phosphoraminimato PR_3 group cone angle was found, with more bulky phosphoraminimate ligands stabilizing the high-spin forms of the complexes and reducing $T_{½}$ [42]. This trend was also reproduced by DF calculations [43].

In each case, trends observed from solid state data on these compounds mirror the solution phase results [29–32,36,38–41,44–47]. Other derivatives of $[Fe(HBpz_3)_2]$ [48–50], $[Fe(terpy)_2]^{2+}$ [51,52] and other complexes in Scheme 4 [53,54] with sterically significant distal ligand substituents also exhibit stabilized high-spin states in solid phases. Interestingly, however, $[Fe(Mes_2\text{-}1\text{-}bpp)_2]^{2+}$ presents an exception to the above discussion, being fully low-spin at room temperature despite the steric bulk of its distal mesityl substituents [39,51]. The increased basicity of the ligand pyrazolyl donors, reflecting the electron-donating character of the mesityl substituents (as opposed to electron-withdrawing phenyl groups), evidently overcomes any steric repulsion in the metal coordination sphere in that example.

Steric effects can also favor the low-spin state, where ligand substituents are oriented to inhibit *lengthening* of the metal–ligand bonds. This is apparent in the [Fe(RB{mpz}$_3$)$_2$] scorpionates (Figure 2), which are high-spin for R = H, pz, *n*Bu, *i*Bu, C_4H_4I-4 or $C_6H_4CCH_4$. However, when R = *t*Bu, the compound is low-spin at 300 K but undergoes gradual SCO upon heating in the solid state [55]. This reflects steric repulsion between the *tert*butyl substituents and the *H*5 atoms on the pyrazolyl rings, which promotes the low-spin state by disfavoring the expanded metal coordination sphere adopted by the high-spin form (Figure 2). Another example is [Fe(Me$_4$-1-bpp)$_2$]$^{2+}$, which contains methyl groups at both the pyrazolyl *C*3 and *C*5 positions. *Intra*-ligand steric repulsion between the *C*5 methyl groups and the pyridyl *H*3/*H*5 atoms also force the pyrazolyl ligand donors closer to the iron atom (Figure 2). Hence [Fe(Me$_4$-1-bpp)$_2$]$^{2+}$ is low-spin [56,57], in contrast to unsubstituted [Fe(1-bpp)$_2$]$^{2+}$ which is SCO-active below room temperature [38]. In both examples the steric influence of pyrazolyl *C*3 methyl groups, which should promote a high-spin state as above, is overcome by a sterically imposed ligand conformation favoring a low-spin structure.

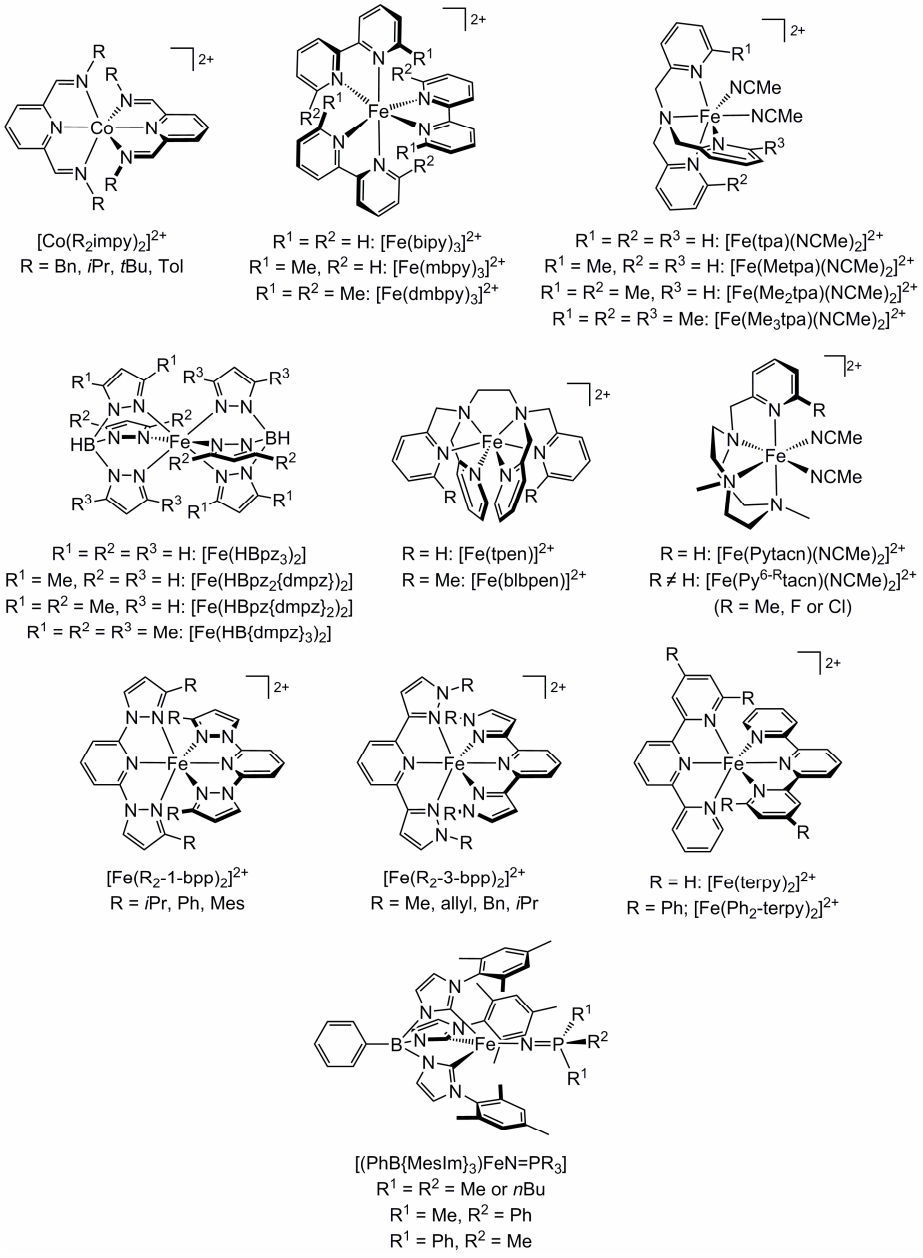

Scheme 4. Complexes whose high-spin state is stabilized by distal ligand substituents.

Steric repulsion can also influence the spin state in framework materials. A good example is provided by $[Fe(3\text{-Xpy})_2\{M(CN)_2\}_2]$ (M = Cu or Au) [58–60], and $[Fe(3\text{-Xpy})_2\{M(CN)_4\}_2]$ (M = Ni, Pd and Pt) [61], where 3-Xpy corresponds to 3-fluoro-, 3-chloro-, 3-bromo-, or 3-iodo-pyridine. Although the members of these series are not perfectly isostructural, they all adopt 2D grid-type topologies with the layers being separated by the 3-halopyridine rings. In each case, the high-spin state of the material is stabilized as the size of the halogen substituent increases, with most 3-bromopyridine frameworks and all the 3-iodopyridine frameworks being high-spin. This was attributed to increased congestion of the inter-layer space in the frameworks as the halogens get larger (Figure 3).

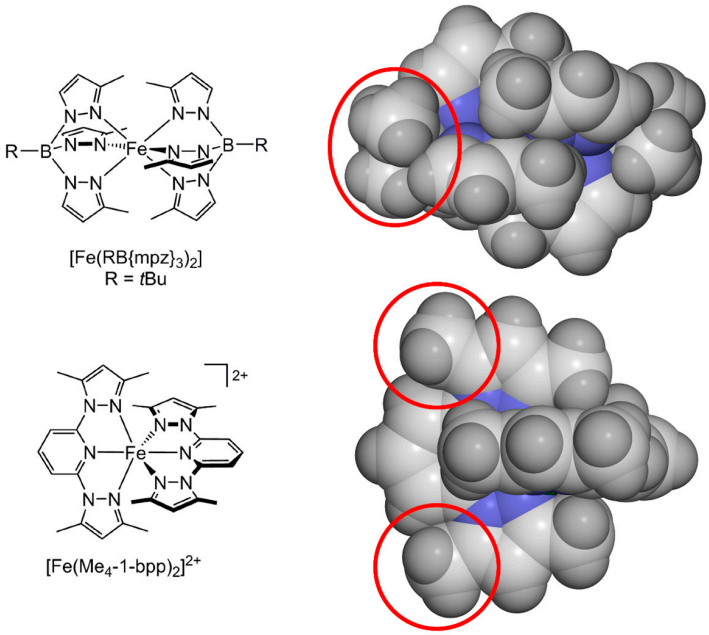

Figure 2. Structures and crystallographic space-filling views of two complexes exhibiting low-spin states stabilized by the highlighted steric repulsions at the periphery of the molecules [55,57]. The orientation of the space-filling views is similar to the structure diagrams. Color code: C, white; H, pale gray; Fe, green; N, blue.

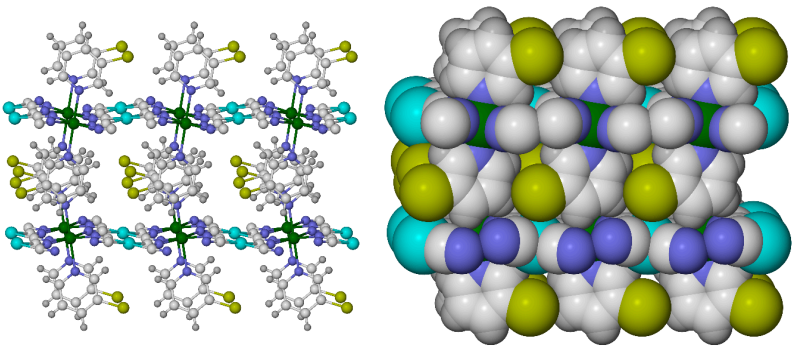

Figure 3. Two views of the 2D Hoffman network $[Fe(3\text{-Brpy})_2\{Pt(CN)_4\}_2]$, plotted from the same orientation [61]. The space-filling view shows the steric influence of the pyridyl bromo substituents in the interlayer space. Color code: C, white; H, pale gray; Br, yellow; Fe, green; N, blue; Pt, cyan.

2.2. *Influence of Ligand Conformation on Metal Ion Spin States*

The high-spin form of a complex can be stabilized by a sterically-induced twisted ligand conformation. The best example is provided by the 3,3′-disubstituted bipyridyl ligand complexes in Scheme 5, where solid salts of $[Fe(3,3'\text{-dmbpy})_2]^{2+}$, $[Fe(dmbc)_2]^{2+}$ and $[Fe(biq)_3]^{2+}$ are all

SCO-active while the parent complex $[Fe(bipy)_3]^{2+}$ is low-spin [31,62]; $[Fe(biq)_3]^{2+}$ also exhibits SCO in solution [31]. This was attributed to twisting of the bipyridyl ligands, induced by an intra-ligand steric clash between the pyridyl substituents, or between the isoquinolinyl *H*8 atoms in coordinated biq. The twisted ligand conformations displace the ligand lone pairs away from the metal–ligand vector, thus weakening the ligand field in the complexes. Such twisting is clear in the crystal structure of $[Fe(3,3'\text{-dmbpy})_2][ClO_4]_2$, where the dihedral angles between the least squares planes of the pyridyl rings in the 3,3′-dmbpy ligands are 36.9–37.1° (Figure 4) [62].

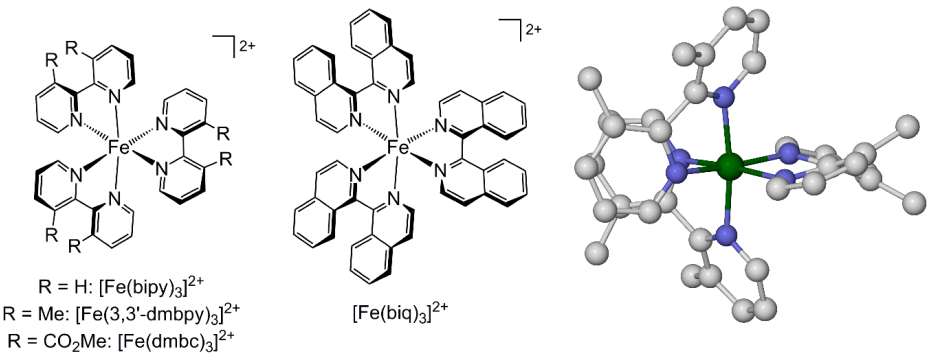

Figure 4. $[Fe(bipy)_3]^{2+}$ derivatives designed to adopt twisted ligand conformations, and the crystal structure of $[Fe(3,3'\text{-dmbpy})_3]^{2+}$ oriented to emphasize the twisting of the bipyridyl framework [62]. Color code: C, white; H, pale gray; Fe, green; N, blue.

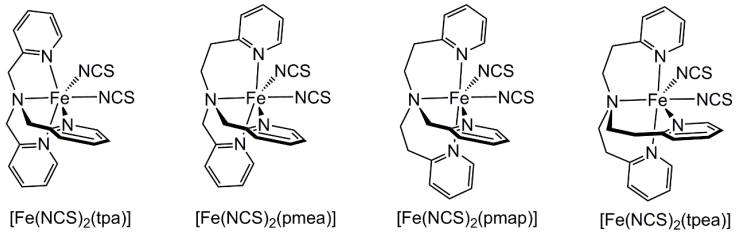

Scheme 5. A series of complexes with sequentially expanded chelate ring sizes.

Another example of the same effect occurs in some *trans*-$[Fe(NCS)_2L]$ complexes, where L represents a series of meridional tetrapyridyl ligands which adopt helically twisted conformations when coordinated to a metal ion. While not all were crystallographically characterized, examples that might be expected to adopt more twisted L ligands are high-spin, or exhibit significantly reduced SCO $T_{½}$ values, in the solid state [63,64]. Comparably distorted ligand conformations, imposed by intermolecular steric contacts rather than by ligand design, may also be responsible for stabilization of the high-spin state in some other crystalline metal complexes [65–70].

2.3. Influence of Chelate and Macrocycle Ring Size on Metal Ion Spin States

Expanded chelate ring sizes should also promote the high spin states of complexes, by increasing the ligand conformational strain associated with the more compact low-spin form [71,72]. Thus, $[Fe(NCS)_2(tpa)]$ [73] and $[Fe(NCS)_2(pmea)]$ [74] are SCO-active with $T_{½}$ between 150 and 220 K, but $[Fe(NCS)_2(pmap)]$ and $[Fe(NCS)_2(tpea)]$ are fully high-spin in the solid state (Scheme 5) [72]. Similar results might be expected in iron(III) complexes of polydentate salicyl Schiff base ligands like salten or saltrien [75,76], for example, although that remains to be confirmed by a solution-phase study. It is harder to elucidate trends from those compounds in the solid state, since their SCO is often very gradual and can be influenced by the salicyl ligand conformation in the crystal [68].

For similar reasons, macrocyclic complexes with larger ring sizes will also tend to favor the expanded coordination sphere in the high-spin state [77]. Although there have been few systematic

studies, an example is provided by a series of iron(II) complexes of a series of hexadentate ligands based on triaza-macrocyclic skeletons with pyridyl pendant arms. These complexes are low-spin for a nine-membered macrocyclic ligand [78], SCO-active in solution for a 10-membered macrocycle [79], and high-spin for a 12-membered macrocycle [78].

2.4. Influence of Ligand Donor Types on Metal Ion Spin State

This is fundamentally a straightforward question, since ligand donors near the top of the spectrochemical series should favor the low-spin state, and *vice versa*. However, most SCO complexes are prepared from a limited palette of ligands, mostly N-donors of different types or mixed N/O-donor chelates. Among the field of SCO complexes, the influence of different types of N- or O-donor on metal ions spin states is more subtle, and harder to quantify from available solution-phase data. On one hand, SCO equilibria in $[Fe(HBpz_3)_2]$ (in thf or a chlorinated solvent [33,34]) and $[Fe(HBtz_3)_2]$ (in D_2O [80]) have both been reported with $T_{½} \approx 330$ K (Scheme 6), which is consistent with the similar basicities of the pyrazole and 1,2,4-triazole heterocycles [81]. In contrast, however, $[Fe(3\text{-bpp})_2]^{2+}$ exhibits SCO with $T_{½} \approx 248$ K in $(CD_3)_2CO$ [5,82], but $[Fe(3\text{-btzp})_2]^{2+}$ remains fully high-spin across the liquid range of that solvent [83] while $[Fe(4\text{-bthp})_2]^{2+}$ is apparently low-spin [84] (Scheme 6). Hence, the identity of the distal heterocyclic donors has a much greater influence on the spin state of complexes with that ligand geometry.

More consistent data are found with azinyl donor heterocycles, in that $[Fe(1\text{-bppyz})_2]^{2+}$ ($T_{½}$ = 268 K in $\{CD_3\}_2CO$ [85]) exhibits a slightly higher temperature SCO than $[Fe(1\text{-bpp})_2]^{2+}$ ($T_{½}$ = 248 K [38]); and, $T_{½}$ for $[Fe(paptz)_2]$ (>300 K in CD_3OD) is also higher than in $[Fe(papt)_2]$ (220 K) [86] (Scheme 6). Thus, replacement of pyridyl by pyrazinyl donors stabilizes the low-spin state of these complexes to a small extent. This is unexpected at first glance, since pyrazine is a less basic heterocycle than pyridine, but it may reflect improved Fe→L backbonding to the more electron-deficient pyrazine heterocycle, as discussed in the next section.

A result relevant to O-donor ligands is that $[Fe(naphtrien)]^+$ ($T_{½}$ = 332 K in $\{CD_3\}_2CO$ [68]) exhibits SCO at slightly higher temperature than $[Fe(saltrien)]^+$ in the same solvent (280 K) [87] (Scheme 6). Since phenol and 2-naphthol have acidic *pK* as of 10.0 and 9.5, respectively, the less basic phenoxide donors in $[Fe(naphtrien)]^+$ are stabilizing the low-spin state in that system. That is consistent with the observed effect of ligand substituents on the spin state of $[Fe(saltrien)]^+$, as again described below. The same trend was observed in the solid state, in these compounds [68] and in another family of iron(III) complexes with pentadentate Schiff base supporting ligands [88].

2.5. Electronic Influence of Ligand Substituents on Metal Ion Spin State—Inductive vs. Resonance Effects

Relatively few studies have been published relating ligand substituents and metal ion spin state, in systems where contamination from steric influences can be excluded. The first report concerned a series of di-iron complexes $[Fe_2(NCE)_2(py^R)_2(\mu\text{-bpypz})_2]$ (E = S or BH_3), where py^R is a 3- or 4-substituted pyridine terminal ligand, which all exhibit comparably gradual thermal SCO in the solid state involving both iron atoms (Scheme 7). Two groups of complexes with thiocyanato or cyanoborohydride co-ligands, each with six different substituted pyridines, show similar positive linear free energy relationships between the pyridine substituent Hammett parameter [89] and the SCO $T_{½}$ [90,91]. That is, more electron-withdrawing pyridine substitutents raise $T_{½}$ and stabilize the low-spin states of the complexes. Similar results were obtained in solution for two series of complexes of polydentate ligands, $[Fe(Py^{4-R}tacn)(NCMe)_2]^{2+}$ [37,92] and $[Fe(stybp^R)_2]^{2+}$ [93] (Scheme 7). In both cases, electron-withdrawing substituents on the 4-pyridyl ligand donors were observed to lower the room temperature magnetic moment or to raise $T_{½}$, both consistent with stabilization of the low-spin state. Collected data from $[Fe(saltrien^R)]^+$ derivatives [68,87], measured in $(CD_3)_2CO$ solution, also afford a positive linear free energy relationship when $T_{½}$ is plotted against the "R" substituent Hammett parameter (Figure 5).

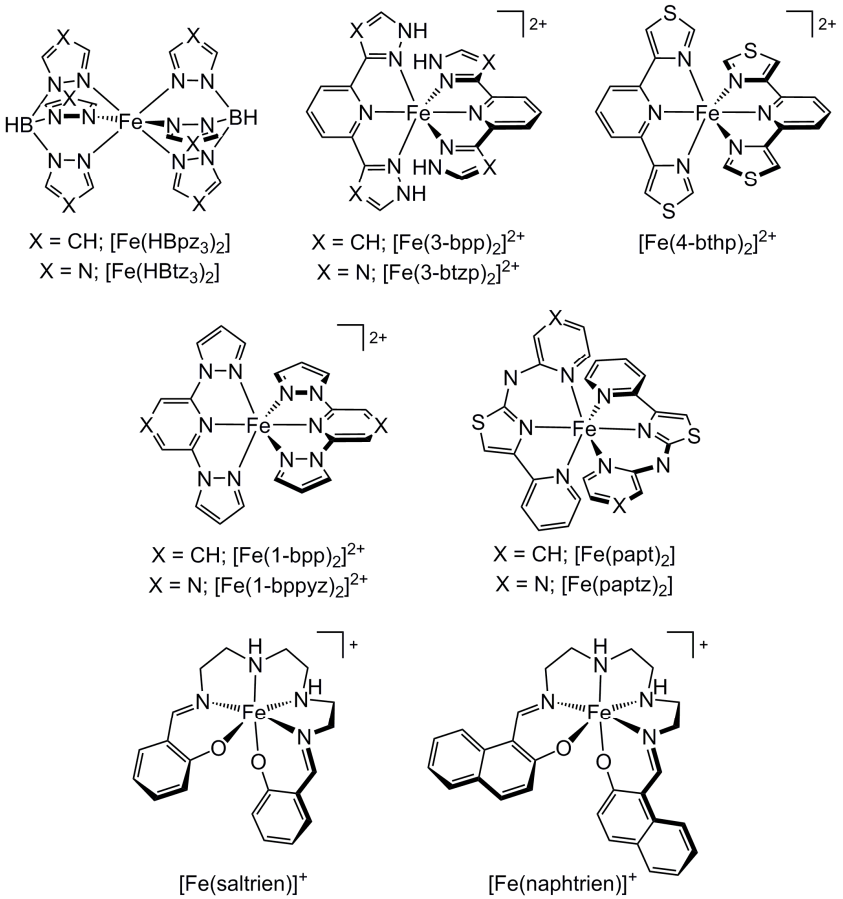

Scheme 6. Comparable complexes, containing different types of heterocyclic N or aromatic O donors, whose SCO has been measured in solution.

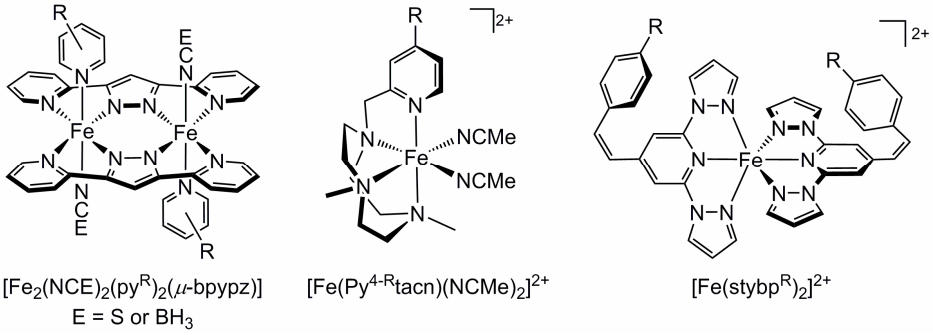

Scheme 7. Three series of complexes whose low-spin state is stabilized by electron-withdrawing pyridyl 'R' substituents in solution [37,90,93].

These results are consistent with those in Section 2.4. Pyridyl groups with electron-withdrawing substituents, and pyrazinyl donors, are both less electron-rich than an unsubstituted pyridyl ring and lead to higher $T_{½}$ values in otherwise identical complexes (Scheme 6). Similarly, a phenoxide donor with an electron-withdrawing substituent, and a more conjugated naphthoxide ring, are less basic than an unsubstituted phenoxide and also act to raise $T_{½}$ in derivatives of $[Fe(saltrien)]^{+}$.

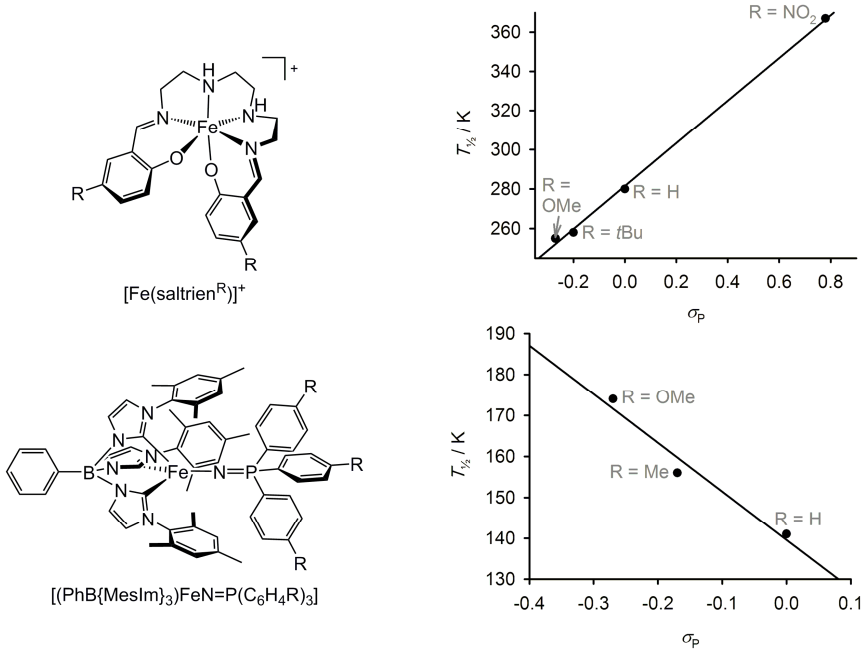

Figure 5. Two families of compounds giving contrasting linear free energy relationships between SCO $T_{½}$ and their ligand 'R' substituent δ_P Hammett parameters from solution measurements [42,68,87].

Conversely, however, some other studies have observed the opposite trend. Most striking are three tetrahedral complexes [(PhB{MesIm}$_3$)FeN=P(C$_6$H$_4$R)$_3$], which afforded a negative free energy relationship between $T_{½}$ and the aryl "R" substitutents in d^8-thf solution (Figure 5) [42]. That is, the low-spin state of these complexes is stabilized by electron-donating, not electron-withdrawing, substituents. Another recent study of different tetrahedral iron(II) complexes [(MeC{CH$_2$PR$^1_2$}$_3$)FeN=PR$^2_3$] (Scheme 8) showed a dependence of $T_{½}$ on both R^1 and R^2, but deconvolution of steric and electronic substituent effects in that series is not so straightforward [94]. However, data from the solid dinuclear complexes [Fe$_2$(tpa)$_2$(μ-dabq^R)][BAr^F]$_2$ showed $T_{½}$ decreasing as the electronegativity of 'R' increases, in the order X = H > Br > Cl > F [95]. That is a similar trend to the [(PhB{MesIm}$_3$)FeN=P(C$_6$H$_4$R)$_3$] system.

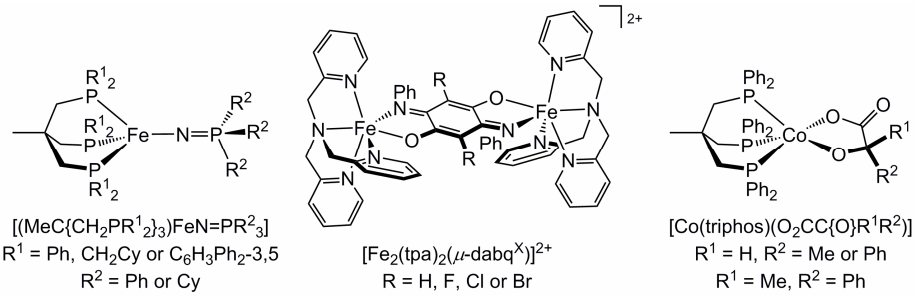

Scheme 8. Other families of substituted complexes with available, comparative SCO data [94–96].

SCO data in methanol solution are also available for three complexes of type [Co(triphos)(O$_2$CC{O}R^{1}R^2)] (Scheme 8). However, their behavior within the liquid range of the solvent is too similar to distinguish any differences between them [96].

The contradictory results described above were reconciled in a recent study of solution-phase SCO data from 24 derivatives of [Fe(1-bpp)$_2$]$^{2+}$ (Figure 6) [97]. Examples bearing pyridyl substituents, [Fe(1-bpp^{R1,H})$_2$]$^{2+}$, showed a positive linear free energy relationship between $T_{½}$ and the substituent R^1, consistent with the complexes in Scheme 7. In contrast, complexes substituted at the pyrazole

donors, $[Fe(1\text{-}bpp^{H,R2})_2]^{2+}$, exhibited a weaker negative linear free energy relationship between $T_{½}$ and the substituent R^2. DFT calculations reproduced that trend, and showed it to reflect a competition between metal–ligand σ- and π-bonding effects.

On one hand, electron-withdrawing substituents reduce the ligand field on inductive grounds, by weakening ligand→metal σ-donation. On the other, electron-withdrawing substituents also lower the energy of the heterocycle π * MOs, which promotes metal–ligand π-back-bonding to strengthen the ligand field. Back-bonding is most important in complexes with 4-substituted pyridyl donors like $[Fe(1\text{-}bpp^{R1,H})_2]^{2+}$, where the substituents are para to the N-donor atom and can conjugate with the metal ion t_{2g} d-orbitals. However, the R^2 substituents in $[Fe(1\text{-}bpp^{H,R2})_2]^{2+}$ are meta to the pyrazolyl N-donors, and are unable to undergo π-conjugation to the metal center. Thus, metal–ligand σ-bonding considerations dominate in the $[Fe(1\text{-}bpp^{H,R2})_2]^{2+}$ series.

Moreover, when only the subset of complexes bearing weakly π-bonding halogen substituents was considered, the $[Fe(1\text{-}bpp^{R1,H})_2]^{2+}$ and $[Fe(1\text{-}bpp^{H,R2})_2]^{2+}$ series instead exhibited identical behavior, with a linear correlation between decreasing $T_{½}$ and increasing halogen electronegativity [97]. That reproduces the trend observed for $[Fe_2(tpa)_2(\mu\text{-}dabq^R)][BAr^F]_2$ (Scheme 8) [95], while emphasizing the importance of π-back-bonding to the behavior of the $[Fe(1\text{-}bpp^{R1,H})_2]^{2+}$ series.

As well as the pyridyl-substituted complexes in Scheme 7, these arguments explain the behavior of $[(PhB\{MesIm\}_3)FeN{=}P(C_6H_4R)_3]$ (Figure 5) whose C_6H_4R substituents cannot conjugate with the iron atom, being separated from it by a sp^3-hybridized P atom. The spin state of the complex would then be governed by the δ-inductive properties of the R substituents, as observed in [42]. The positive linear free energy relationship for $[Fe(saltrien^R)]^+$ (Figure 5) also implies that iron/phenoxide π-bonding is important to those compounds. In that case, electron-withdrawing substituents would strengthen the ligand field by reducing ligand–metal π-donation.

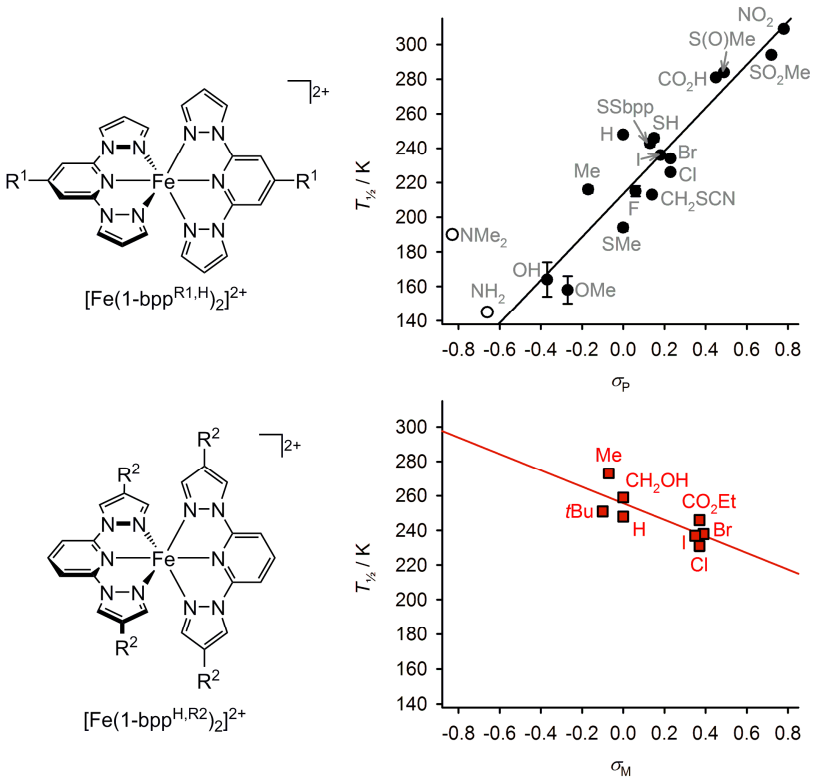

Figure 6. Linear SCO free energy relationships for $[Fe(1\text{-}bpp)_2]^{2+}$ bearing pyridyl R^1 (black circles) and pyrazolyl R^2 (**red squares**) substituents. Data were measured in $(CD_3)_2CO$ or CD_3NO_2 solution [97]. The data points for $R^1 = NH_2$ and NMe_2 (**white circles**) represent upper limits for those $T_{½}$ values, since those complexes remained fully high-spin within the liquid range of the solvent used.

Surprisingly, derivatives of $[Fe(3\text{-bpp})_2]^{2+}$ (Scheme 2) substituted at the pyrazolyl C5 positions did not follow the same trends as for $[Fe(1\text{-bpp}^{H,R2})_2]^{2+}$, since in that study both electron-donating and -withdrawing substituents led to a similar reduction in $T_{½}$ [98]. It may be relevant that those pyrazolyl substituents are adjacent to the 3-bpp NH groups, which could lead to them influencing hydrogen bonding by these groups. Hydrogen bonding by $[Fe(3\text{-bpp})_2]^{2+}$ has a strong bearing on its SCO, as described in the next section.

2.6. Effect of Secondary Bonding Interactions on Metal Ion Spin State—Hydrogen Bonding

While data from the solid state are inconclusive [19], solution-phase studies have demonstrated that donation of hydrogen bonds by a coordinated ligand acts to strengthen the ligand field in a complex. For example, SCO measurements of $[Fe(3\text{-bpp})_2]^{2+}$ (Scheme 2) [5], $[Fe(tacn)_2]^{2+}$ [99], $[Fe(pic)_3]^{2+}$ [100] and $[Fe(bzimpy)_2]^{2+}$ (Scheme 9) [101] all afforded increased $T_{½}$ values in more associating solvents. Where it was measured, the highest $T_{½}$ was always obtained in pure water [5,99,100]. The effect was strongest in $[Fe(3\text{-bpp})_2]^{2+}$, where $T_{½}$ in D_2O (317 K) is 60–70 K higher than in six organic solvents (244–257 K) [5,6]. This was attributed to the more polar pyrazolyl NH groups in 3-bpp, which should form stronger hydrogen bonds than the less acidic amino NH groups in tacn or pic [5]. The same trend was noted in the room temperature magnetic moment of $[Fe(saltrien)]^+$, which is reduced in organic solvents of greater donor number (indicating a greater low-spin population) [87].

Hydrogen bonding to anions has a comparable effect on a complex's spin state. This has been best studied in a series of complexes $[Fe(bip)_2L]^{2+}$, where L = bip, bipy or another di-imine co-ligand (Scheme 9). Each bip ligand contains two peripheral NH groups oriented to form chelating N–H···X^- hydrogen bonds to an X^- anion guest [102–105]. Titrating halide or other more associating anions into chloroform solutions of $[Fe(bip)_2L][BPh_4]_2$, around the SCO temperature for each complex, causes a steady high→low spin conversion associated with anion binding to the bip ligands. A comparable effect was also noted in different salts of $[Fe(3\text{-bpp})_2]^{2+}$ (Scheme 2), whose SCO was shifted by up to 15 K higher temperature in the presence of more associating counterions, at NMR concentrations in a 9:1 $(CD_3)_2CO$:D_2O solvent mixture [106]. While studies of $[Fe(tacn)_2]^{2+}$ [99] or $[Fe(pic)_3]^{2+}$ [100] reported no measurable response to different anions in solution, that might reflect the aqueous solvents used for those measurements, which would disfavor intermolecular hydrogen-bonding and ion pairing [107].

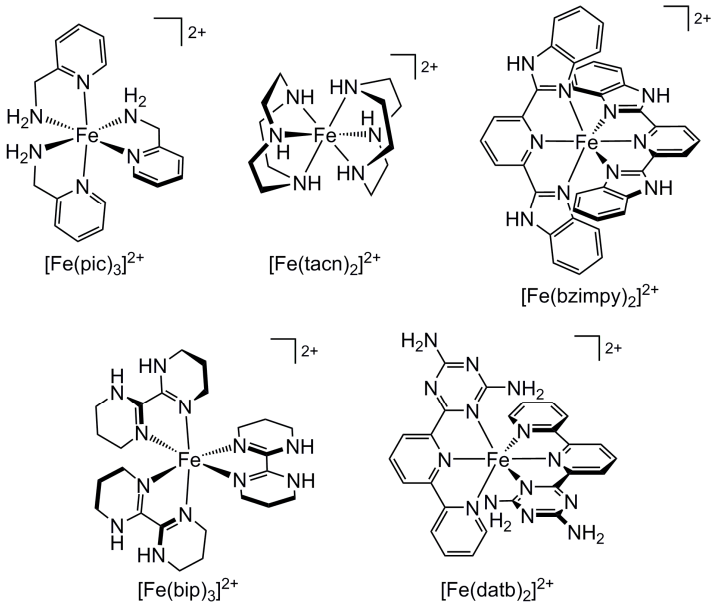

Scheme 9. Complexes with peripheral NH functionality that show a response between hydrogen bond formation and metal ion spin state. See also $[Fe(3\text{-bpp})_2]^{2+}$ (Scheme 2).

Although these results have yet to be addressed computationally, it is reasonable that formation of an N–H···X hydrogen bond to an anion or solvent should increase the dipole on the $N^{\delta-}$–$H^{\delta+}$ group. That would make the ligand more electron-rich and more basic, thus increasing the ligand field, as observed. The converse effect on $T_{½}$, of guest-binding to a hydrogen-bond acceptor ligand site, has not yet been studied systematically. However, it is noteworthy that binding of barbiturate derivatives to $[Fe(datb)_2]^{2+}$ causes a low→high spin state change, the opposite of the other compounds in this section [108,109]. The 4,6-diaminotriazinyl receptor sites in $[Fe(datb)_2]^{2+}$ contain a mixture of hydrogen bond donor and receptor functions, making the interaction between substrate binding and spin state harder to rationalize in that system.

3. Materials and Methods

Crystallographic figures in this article were prepared with *XSeed* [110], using coordinates obtained from the Cambridge Crystallographic Database [111], and graphs were generated using *SigmaPlot* [112].

4. Conclusions

The steric aspects of ligand design for control of metal ion spin state are clear cut. Bulky substituents in the vicinity of the ligand donor atoms, expanded ligand chelate ring structures, or any other factor that disfavors contraction of the metal–ligand bonds will stabilize the high-spin state of a complex. Steric bulk at the periphery of the ligand sphere can promote the low-spin state if it inhibits expansion of the metal coordination sphere, or the high-spin state if it leads to distortion of the ligand→metal dative interaction. These effects can be reliably understood or predicted in individual compounds computationally [43,50,92] or using molecular models.

The response of a complex's spin state to changes in the electronic structure of its ligands is more subtle, and requires further study. Remote electron-withdrawing substituents can promote either the high-spin or the low-spin state, depending on two factors: the π-bonding character of the substituent, as expressed by its Hammett parameter [89]; and its position on the ligand framework, which influences the ability of the substituent to conjugate to the metal t_{2g} orbitals [97]. For heterocyclic ligand donors, this can be predicted using physical organic chemistry principles: substituents *ortho* or *para* to a reaction center (ligand donor/metal ion) can conjugate to it, but *meta* substituents cannot.

Finally, the modulation of spin state through supramolecular host:guest binding offers an attractive route to reporter groups for molecular sensors, for example. There are enough proofs-of-principle for a consistent result to emerge that ligands with peripheral NH groups exert an increased ligand field when engaged in strong hydrogen bonding interactions. However, the literature also contains more complicated examples that do not follow that simple trend [98,108], and the synthesis of new supramolecular SCO systems could shed new light on this complicated question.

Acknowledgments: My own work in this area has been supported by the EPSRC (EP/H015639/1, EP/K012568/1), the University of Leeds, and the COST network CM1305 Explicit Control of Spin States in Technology and Biology (ECOSTBio). The author thanks Laurence Kershaw Cook and Rafal Kulmaczewski (University of Leeds), Rob Deeth (University of Edinburgh), and other collaborators mentioned in the reference list for their contributions.

Conflicts of Interest: The author declares no conflict of interest.

Abbreviations

The following abbreviations are used in this manuscript:

1-bpp	2,6-di{pyrazol-1-yl}pyridine
1-bppyz	2,6-di{pyrazol-1-yl}pyrazine
3-bpp	2,6-di{1*H*-pyrazol-3-yl}pyridine
3-btzp	2,6-di{1*H*-1,2,4-triazol-3-yl}pyridine
3,3′-dmbpy	3,3′-dimethyl-2,2′-bipyridine
4-bthp	2,6-di{thiazol-4-yl}pyridine
$BArF^-$	*tetrakis*(3,5-di{trifluoromethyl}phenyl)borate
Bip	2,2′-bi(1,4,5,6-tetrahydropyrimidine)

bipy	2,2′-bipyridine
biq	2,2′-bi(*iso*)quinoline
blbpen	*N N′-bis*(6-methylpyrid-2-ylmethyl)-*N*,*N′-bis*(pyrid-2-ylmethyl)-1,2-diaminoethane
Bn	benzyl
bpypzH	3,5-di(pyrid-2-yl)-1*H*-pyrazole
bzimpy	2,6-*bis*(1*H*-benzimidazol-2-yl)pyridine
Cy	cyclohexyl
dabqH_2	2,5-(phenylamino)-1,4-benzoquinone
dmbc	dimethyl 2,2'-bipyridine-3,3'-dicarboxylate
dmbpy	6,6′-dimethyl-2,2′-bipyridine
dmpz	3,5-dimethylpyrazol-1-yl
impy	2,6-*bis*(carbaldimino)pyridine
*i*Pr	*iso*propyl
mbpy	6-methyl-2,2′-bipyridine
Me	methyl
MeCN	acetonitrile
MePy$_3$tren	*bis*(4-{pyrid-2-yl}-3-aza-3-butenyl)(4-{6-methylpyrid-2-yl}-3-aza-3-butenyl)amine
Me$_2$Py$_3$tren	(4-{pyrid-2-yl}-3-aza-3-butenyl)-*bis*-(4-{6-methylpyrid-2-yl}-3-aza-3-butenyl)amine
Me$_3$Py$_3$tren	*tris*(4-{6-methylpyrid-2-yl}-3-aza-3-butenyl)amine
MesIm	3-(2,4,6-trimethylphenyl)imidazol-1-yl
Metpa	*bis*(pyrid-2-ylmethyl)({6-methylpyrid-2-yl}methyl)amine
Me$_2$tpa	(pyrid-2-ylmethyl)-*bis*({6-methylpyrid-2-yl}methyl)amine
Me$_3$tpa	*tris*({6-methylpyrid-2-yl}methyl)amine
Mes	mesityl, 2,4,6-triphenylphenyl
Mpz	3-methylpyrazol-1-yl
naphtrienH_2	1,8-*bis*(2-hydroxynaphthaldiminato)-3,6-diazaoctane
paptH	2-(pyrid-2-y1amino)-4-(pyridin-2-yl)thiazole
Ph	phenyl
Pic	2-(aminomethyl)pyridine, 2-picolylamine
Pmap	(pyrid-2-ylmethyl)-*bis*(2-{pyrid-2-yl}ethyl)amine
Pmea	*bis*(pyrid-2-ylmethyl)(2-{pyrid-2-yl}ethyl)amine
Pytacn	1-(pyrid-2-ylmethyl)-4,7-dimethyl-1,4,7-triazacyclononane
Py$_3$tren	*tris*(4-{pyrid-2-yl}-3-aza-3-butenyl)amine
Py	pyridine
pz	pyrazol-1-yl
pzaptH	2-(pyrazin-2-y1amino)-4-(pyridin-2-yl)thiazole
saltenH_2	1,7-*bis*(salicylaldiminato)-4-azaheptane
saltrienH_2	1,8-*bis*(salicylaldiminato)-3,6-diazaoctane
stybp	4-(*cis*-styryl)-2,6-di(pyrazol-1-yl)pyridine
SCO	Spin crossover
Tacn	1,4,7-triazacyclononane
*t*Bu	*tert*butyl
thf	etrahydrofuran
Tol	4-methylphenyl, 4-tolyl
Tpa	*tris*(pyrid-2-ylmethyl)amine
tpea	*tris*(2-{pyrid-2-yl}ethyl)amine
tpen	*N*,*N*,*N′*,*N′-tetrakis*-(pyrid-2-ylmethyl)-1,2-diaminoethane
triphos	1,1,1-*tris*(diphenylphosphinomethyl)ethane.

References

1. Weller, M.; Overton, T.; Rourke, J.; Armstrong, F. *Inorganic Chemistry*, 6th ed.; Oxford University Press: Oxford, UK, 2014; pp. 515–549.
2. O'Connor, C.J. Magnetochemistry—Theory and experiment. *Prog. Inorg. Chem.* **1982**, *29*, 203–283.
3. Swart, M., Costas, M. (Eds.) *Spin States in Biochemistry and Inorganic Chemistry: Influence on Structure and Reactivity*; John Wiley & Sons: Chichester, UK, 2016; p. 465.
4. Andris, E.; Jašík, J.; Gomez, L.; Costas, M.; Roithová, J. Spectroscopic characterization and reactivity of triplet and quintet iron(IV)-oxo complexes in the gas phase. *Angew. Chem. Int. Ed.* **2016**, *55*, 3637–3641. [CrossRef] [PubMed]
5. Barrett, S.A.; Kilner, C.A.; Halcrow, M.A. Spin-crossover in [Fe(3-bpp)$_2$][BF$_4$]$_2$ in different solvents—A dramatic stabilisation of the low-spin state in water. *Dalton Trans.* **2011**, *40*, 12021–12024. [CrossRef] [PubMed]
6. Jeon, I.-R.; Park, J.G.; Haney, C.R.; Harris, T.D. Spin crossover iron(II) complexes as PARACEST MRI thermometers. *Chem. Sci.* **2014**, *5*, 2461–2465. [CrossRef]

7. Harvey, J.N.; Poli, R.; Smith, K.M. Understanding the reactivity of transition metal complexes involving multiple spin states. *Coord. Chem. Rev.* **2003**, *238–239*, 347–361. [CrossRef]
8. Ye, S.; Geng, C.-Y.; Shaik, S.; Neese, F. Electronic structure analysis of multistate reactivity in transition metal catalyzed reactions: The case of C–H bond activation by non-heme iron(IV)-oxo cores. *Phys. Chem. Chem. Phys.* **2013**, *15*, 8017–8030. [CrossRef] [PubMed]
9. Poulos, T.L. Heme enzyme structure and function. *Chem. Rev.* **2014**, *114*, 3919–3962. [CrossRef] [PubMed]
10. Nam, W.; Lee, Y.-M.; Fukuzumi, S. Tuning reactivity and mechanism in oxidation reactions by mononuclear nonheme iron(IV)-oxo complexes. *Acc. Chem. Res.* **2014**, *47*, 1146–1154. [CrossRef] [PubMed]
11. Puri, M.; Que, L., Jr. Toward the synthesis of more reactive S = 2 non-heme oxo-iron(IV) complexes. *Acc. Chem. Res.* **2015**, *48*, 2443–2452. [CrossRef] [PubMed]
12. Holland, P.L. Distinctive reaction pathways at base metals in high-spin organometallic catalysts. *Acc. Chem. Res.* **2015**, *48*, 1696–1702. [CrossRef] [PubMed]
13. Shaver, M.P.; Allan, L.E.N.; Rzepa, H.S.; Gibson, V.C. Correlation of metal spin state with catalytic reactivity: Polymerizations mediated by α-diimine–iron complexes. *Angew. Chem. Int. Ed.* **2006**, *45*, 1241–1244. [CrossRef] [PubMed]
14. Johansson, M.P.; Swart, M. Subtle effects control the polymerisation mechanism in α-diimine iron catalysts. *Dalton Trans.* **2011**, *40*, 8419–8428. [CrossRef] [PubMed]
15. Halcrow, M.A. (Ed.) *Spin-Crossover Materials—Properties and Applications*; John Wiley & Sons: Chichester, UK, 2013; p. 568.
16. Bousseksou, A.; Molnár, G.; Salmon, L.; Nicolazzi, W. Molecular spin crossover phenomenon: Recent achievements and prospects. *Chem. Soc. Rev.* **2011**, *40*, 3313–3335. [CrossRef] [PubMed]
17. Gütlich, P.; Gaspar, A.B.; Garcia, Y. Spin state switching in iron coordination compounds. *Beilstein J. Org. Chem.* **2013**, *9*, 342–391. [CrossRef] [PubMed]
18. Toftlund, H. Spin equilibrium in solutions. *Monatsh. Chem.* **2001**, *132*, 1269–1277. [CrossRef]
19. Halcrow, M.A. Structure: Function relationships in molecular spin-crossover complexes. *Chem. Soc. Rev.* **2011**, *40*, 4119–4142. [CrossRef] [PubMed]
20. Kahn, O.; Krober, J.; Jay, C. Spin transition molecular materials for displays and data recording. *Adv. Mater.* **1992**, *4*, 718–728. [CrossRef]
21. Manrique-Juárez, M.D.; Rat, S.; Salmon, L.; Molnár, G.; Quintero, C.M.; Nicu, L.; Shepherd, H.J.; Bousseksou, A. Switchable molecule-based materials for micro- and nanoscale actuating applications: Achievements and prospects. *Coord. Chem. Rev.* **2016**, *308*, 395–408. [CrossRef]
22. Cavallini, M. Status and perspectives in thin films and patterning of spin crossover compounds. *Phys. Chem. Chem. Phys.* **2012**, *14*, 11867–11876. [CrossRef] [PubMed]
23. Hassan, N.; Koudriavtsev, A.B.; Linert, W. Isoequilibrium relationships and cooperative effects in spin-state transitions in solution. *Pure Appl. Chem.* **2008**, *80*, 1281–1292. [CrossRef]
24. König, E. Structural changes accompanying continuous and discontinuous spin-state transitions. *Prog. Inorg. Chem.* **1987**, *35*, 527–622.
25. Hoselton, M.A.; Wilson, L.J.; Drago, R.S. Substituent effects on the spin equilibrium observed with hexadentate ligands on iron(II). *J. Am. Chem. Soc.* **1975**, *97*, 1722–1729. [CrossRef]
26. Seredyuk, M.; Gaspar, A.B.; Ksenofontov, V.; Galyametdinov, Y.; Kusz, J.; Gütlich, P. Does the solid-liquid crystal phase transition provoke the spin-state change in spin-crossover metallomesogens? *J. Am. Chem. Soc.* **2008**, *130*, 1431–1439. [CrossRef] [PubMed]
27. Brewer, G.; Luckett, C.; May, L.; Beatty, A.M.; Scheidt, W.R. Synthesis and characterization of tripodal iron(II) complexes prepared from 2-pyridinecarboxaldehyde and 1-methyl-2-imidazolecarboxaldehyde: Stabilization of iron(II) cations with N_6 donor sets. *Inorg. Chim. Acta* **2004**, *357*, 2390–2396. [CrossRef]
28. Seredyuk, M.; Gaspar, A.B.; Kusz, J.; Bednarek, G.; Gütlich, P. Variable-temperature X-ray crystal structure determinations of {Fe[tren(6-Mepy)$_3$]}(ClO$_4$)$_2$ and {Zn[tren(6-Mepy)$_3$]}(ClO$_4$)$_2$ compounds: Correlation of the structural data with magnetic and Mössbauer spectroscopy data. *J. Appl. Cryst.* **2007**, *40*, 1135–1145. [CrossRef]
29. Simmons, M.G.; Wilson, L.J. Magnetic and spin lifetime studies in solution of a ΔS = 1 spin-equilibrium process for some six-coordinate bis(*N*-R-2,6-pyridinedicarboxaldimine)cobalt(II) complexes. *Inorg. Chem.* **1977**, *16*, 126–130. [CrossRef]

30. Onggo, D.; Hook, J.M.; Rae, A.D.; Goodwin, H.A. The influence of steric effects in substituted 2,2′-bipyridine on the spin state of iron(II) in $[FeN_6]^{2+}$ systems. *Inorg. Chim. Acta* **1990**, *173*, 19–30. [CrossRef]
31. Onggo, D.; Goodwin, H.A. Steric effects of the spin state of iron(II) in complexes of substituted bipyridine derivatives. *Aust. J. Chem.* **1991**, *44*, 1539–1551. [CrossRef]
32. Zang, Y.; Kim, J.; Dong, Y.; Wilkinson, E.C.; Appelman, E.H.; Que, L., Jr. Models for nonheme iron intermediates: Structural basis for tuning the spin states of Fe(tpa) complexes. *J. Am. Chem. Soc.* **1997**, *119*, 4197–4205. [CrossRef]
33. Jesson, J.P.; Trofimenko, S.; Eaton, D.R. Spin equilibria in octahedral iron(II) poly(1-pyrazolyl) borates. *J. Am. Chem. Soc.* **1967**, *89*, 3158–3164. [CrossRef]
34. Beattie, J.K.; Binstead, R.A.; West, R.J. Intersystem crossing observed by ultrasonic relaxation of the singlet-quintet spin equilibrium of iron(II) complexes in solution. *J. Am. Chem. Soc.* **1978**, *100*, 3044–3050. [CrossRef]
35. Buchen, T.; Gütlich, P. Substituent effects on the spin equilibrium in iron(II) pyrazolylborate complexes. *Inorg. Chim. Acta* **1995**, *231*, 221–223. [CrossRef]
36. Toftlund, H. Spin equilibria in octahedral iron(II) complexes. *Coord. Chem. Rev.* **1989**, *94*, 67–108. [CrossRef]
37. Prat, I.; Company, A.; Corona, T.; Parella, T.; Ribas, X.; Costas, M. Assessing the impact of electronic and steric tuning of the ligand in the spin state and catalytic oxidation ability of the Fe^{II}(Pytacn) family of complexes. *Inorg. Chem.* **2013**, *52*, 9229–9244. [CrossRef] [PubMed]
38. Holland, J.M.; McAllister, J.A.; Kilner, C.A.; Thornton-Pett, M.; Bridgeman, A.J.; Halcrow, M.A. Stereochemical effects on the spin-state transition shown by salts of $[FeL_2]$ [L = 2,6-di(pyrazol-1-yl)-pyridine]. *J. Chem. Soc. Dalton Trans.* **2002**, 548–554. [CrossRef]
39. Holland, J.M.; Barrett, S.A.; Kilner, C.A.; Halcrow, M.A. Control of the spin state of Fe(II) 2,6-di(pyrazol-1-yl)pyridine complexes by distal ligand substitution. *Inorg. Chem. Commun.* **2002**, *5*, 328–332. [CrossRef]
40. Roberts, T.D.; Little, M.A.; Kershaw Cook, L.J.; Barrett, S.A.; Tuna, F.; Halcrow, M.A. Iron(II) complexes of 2,6-di(1-alkylpyrazol-3-yl)pyridine derivatives—The influence of distal substituents on the spin state of the iron center. *Polyhedron* **2013**, *64*, 4–12. [CrossRef]
41. Constable, E.C.; Baum, G.; Bill, E.; Dyson, R.; van Eldik, R.; Fenske, D.; Kaderli, S.; Morris, D.; Neubrand, A.; Neuberger, M.; *et al.* Control of iron(II) spin states in 2,2′:6′,2′′-terpyridine complexes through ligand substitution. *Chem. Eur. J.* **1999**, *5*, 498–508. [CrossRef]
42. Lin, H.-J.; Siretanu, D.; Dickie, D.A.; Subedi, D.; Scepaniak, J.J.; Mitcov, D.; Clérac, R.; Smith, J.M. Steric and electronic control of the spin state in three-fold symmetric, four-coordinate iron(II) complexes. *J. Am. Chem. Soc.* **2014**, *136*, 13326–13332. [CrossRef] [PubMed]
43. Cirera, J.; Ruiz, E. Theoretical modeling of the ligand-tuning effect over the transition temperature in four-coordinated Fe^{II} molecules. *Inorg. Chem.* **2016**, *55*, 1657–1663. [CrossRef] [PubMed]
44. Jesson, J.P.; Weiher, J.F.; Trofimenko, S. Mössbauer and magnetic susceptibility investigation of the $^5T_2$–$^1A_1$ crossover in some octahedral ferrous complexes in the solid state. *J. Chem. Phys.* **1968**, *48*, 2058–2066. [CrossRef]
45. Oliver, J.D.; Mullica, D.F.; Hutchinson, B.B.; Milligan, W.O. Iron-nitrogen bond lengths in low-spin and high-spin iron(II) complexes with poly(pyrazolyl) borate ligands. *Inorg. Chem.* **1980**, *19*, 165–169. [CrossRef]
46. Elhaïk, J.; Evans, D.J.; Kilner, C.A.; Halcrow, M.A. A structural, magnetic and Mössbauer spectroscopic study of an unusual angular Jahn-Teller distortion in a series of high-spin iron(II) complexes. *Dalton Trans.* **2005**, *9*, 1693–1700. [CrossRef] [PubMed]
47. Luo, Y.-H.; Yang, L.-J.; Liu, Q.-L.; Ling, Y.; Wang, W.; Sun, B.-W. Lattice water molecules tuned spin-crossover for an iron(II) complex with thermal hysteresis. *Dalton Trans.* **2014**, *43*, 16937–16942. [CrossRef] [PubMed]
48. Eichhorn, D.M.; Armstrong, W.H. M{hydrotris(3-phenylpyrazol-l-yl)borate}$_2$: Sterically encumbered iron(II) and manganese(II) complexes. *Inorg. Chem.* **1990**, *29*, 3607–3612. [CrossRef]
49. Cecchi, P.; Berrettoni, M.; Giorgetti, M.; Lobbia, G.G.; Calogero, S.; Stievano, L. The effect of the 3-trifluoromethyl substituent in polypyrazolylborato complexes on the iron(II) spin state; X-ray diffraction and absorption and Mössbauer studies. *Inorg. Chim. Acta* **2001**, *318*, 67–76. [CrossRef]
50. Gruden-Pavlović, M.; Stepanović, S.; Perić, M.; Güell, M.; Swart, M. A density functional study of the spin state energetics of polypyrazolylborato complexes of first-row transition metals. *Phys. Chem. Chem. Phys.* **2014**, *16*, 14514–14522. [CrossRef] [PubMed]

51. Pelascini, F.; Wesolek, M.; Peruch, F.; De Cian, A.; Kyritsaka, N.; Lutz, P.J.; Kress, J. Iron complexes of terdentate nitrogen ligands: Formation and X-ray structure of three new dicationic complexes. *Polyhedron* **2004**, *23*, 3193–3199. [CrossRef]
52. Brauchli, S.Y.; Constable, E.C.; Harris, K.; Häussinger, D.; Housecroft, C.E.; Rösel, P.J.; Zampese, J.A. Towards catenanes using π-stacking interactions and their influence on the spin-state of a bis(2,2′:6′,2′′-terpyridine)iron(II) domain. *Dalton Trans.* **2010**, *39*, 10739–10748. [CrossRef] [PubMed]
53. Halcrow, M.A. The spin-states and spin-transitions of mononuclear iron(II) complexes of nitrogen-donor ligands. *Polyhedron* **2007**, *26*, 3523–3576. [CrossRef]
54. Kisslinger, S.; Kelm, H.; Zheng, S.; Beitat, A.; Würtele, C.; Wortmann, R.; Bonnet, S.; Herres-Pawlis, S.; Krüger, H.-J.; Schindler, S. Synthesis and characterization of iron(II) thiocyanate complexes with derivatives of the tris(pyridine-2-ylmethyl)amine (tmpa) ligand. *Z. Anorg. Allg. Chem.* **2012**, *638*, 2069–2077. [CrossRef]
55. Hamon, P.; Thépot, J.-Y.; le Floch, M.; Boulon, M.-E.; Cador, O.; Golhen, S.; Ouahab, L.; Fadel, L.; Saillard, J.-Y.; Hamon, J.-R. Dramatic remote substitutent effects on the electronic spin state of bis(scorpionate) iron(II) complexes. *Angew. Chem. Int. Ed.* **2008**, *47*, 8687–8691. [CrossRef] [PubMed]
56. Halcrow, M.A. Iron(II) complexes of 2,6-di(pyrazol-1-yl)pyridines—A versatile system for spin-crossover research. *Coord. Chem. Rev.* **2009**, *253*, 2493–2514. [CrossRef]
57. Mohammed, R. Iron Complexes of New Dipyrazolylpyridine Derivatives for Spin-Crossover Applications. Ph.D. Thesis, University of Leeds, Leeds, UK, 2012.
58. Muñoz, M.C.; Gaspar, A.B.; Galet, A.; Real, J.A. Spin-crossover behavior in cyanide-bridged iron(II)-silver(I) bimetallic 2D Hofmann-like metal-organic frameworks. *Inorg. Chem.* **2007**, *46*, 8182–8192. [CrossRef] [PubMed]
59. Agustí, G.; Muñoz, M.C.; Gaspar, A.B.; Real, J.A. Spin-crossover behavior in cyanide-bridged iron(II)-gold(I) bimetallic 2D Hofmann-like metal-organic frameworks. *Inorg. Chem.* **2008**, *47*, 2552–2561. [CrossRef] [PubMed]
60. Agustí, G.; Muñoz, M.C.; Gaspar, A.B.; Real, J.A. Spin-crossover behavior in cyanide-bridged iron(II)-copper(I) bimetallic 1–3D metal-organic frameworks. *Inorg. Chem.* **2009**, *48*, 3371–3381. [CrossRef] [PubMed]
61. Martínez, V.; Gaspar, A.B.; Muñoz, M.C.; Bukin, G.V.; Levchenko, G.; Real, J.A. Synthesis and characterisation of a new series of bistable iron(II) spin-crossover 2D metal-organic frameworks. *Chem. Eur. J.* **2009**, *15*, 10960–10971. [CrossRef] [PubMed]
62. Craig, D.C.; Goodwin, H.A.; Onggo, D. Steric influences on the ground state of iron(II) in the tris(3,3′-dimethyl-2,2′-bipyridine)iron(II) ion. *Aust. J. Chem.* **1988**, *41*, 1157–1169. [CrossRef]
63. Arcis-Castíllo, Z.; Zheng, S.; Siegler, M.A.; Roubeau, O.; Bedoui, S.; Bonnet, S. Tuning the transition temperature and cooperativity of bapbpy-based mononuclear spin-crossover compounds: Interplay between molecular and crystal engineering. *Chem. Eur. J.* **2011**, *17*, 14826–14836. [CrossRef] [PubMed]
64. Zheng, S.; Reintjens, N.R.M.; Siegler, M.A.; Roubeau, O.; Bouwman, E.; Rudavskyi, A.; Havenith, R.W.A.; Bonnet, S. Stabilization of the low-spin state in a mononuclear iron(II) complex and high-temperature cooperative spin crossover mediated by hydrogen bonding. *Chem. Eur. J.* **2016**, *22*, 331–339. [CrossRef] [PubMed]
65. Reger, D.L.; Little, C.A.; Smith, M.D.; Rheingold, A.L.; Lam, K.-C.; Concolino, T.L.; Long, G.J.; Hermann, R.P.; Grandjean, F. Synthetic, structural, magnetic, and Mössbauer spectral study of $[Fe\{HC(3,5\text{-}Me_2pz)_3\}_2]I_2$ and its spin-state crossover behavior. *Eur. J. Inorg. Chem.* **2002**, *2002*, 1190–1197. [CrossRef]
66. Reger, D.L.; Gardinier, J.R.; Elgin, J.D.; Smith, M.D.; Hautot, D.; Long, G.J.; Grandjean, F. Structure-function correlations in iron(II) tris(pyrazolyl)borate spin-state crossover complexes. *Inorg. Chem.* **2006**, *45*, 8862–8875. [CrossRef] [PubMed]
67. Elhaïk, J.; Kilner, C.A.; Halcrow, M.A. Structural diversity in iron(II) complexes of 2,6-di(pyrazol-1-yl)-pyridine and 2,6-di(3-methylpyrazol-1-yl)pyridine. *Dalton Trans.* **2006**, *6*, 823–830. [CrossRef] [PubMed]
68. Pritchard, R.; Barrett, S.A.; Kilner, C.A.; Halcrow, M.A. The influence of ligand conformation on the thermal spin transitions in iron(III) saltrien complexes. *Dalton Trans.* **2008**, 3159–3168. [CrossRef] [PubMed]
69. Kershaw Cook, L.J.; Tuna, F.; Halcrow, M.A. Iron(II) and cobalt(II) complexes of tris-azinyl analogues of 2,2′:6′,2′′-terpyridine. *Dalton Trans.* **2013**, *42*, 2254–2265. [CrossRef] [PubMed]
70. Sertphon, D.; Harding, D.J.; Harding, P.; Murray, K.S.; Moubaraki, B.; Adams, H. Steric trapping of the high spin state in Fe^{III} quinolylsalicylaldimine complexes. *Aust. J. Chem.* **2014**, *67*, 1574–1580. [CrossRef]

71. Matouzenko, G.S.; Borshch, S.A.; Jeanneau, E.; Bushuev, M.B. Spin crossover in a family of iron(II) complexes with hexadentate ligands: Ligand strain as a factor determining the transition temperature. *Chem. Eur. J.* **2009**, *15*, 1252–1260. [CrossRef] [PubMed]
72. Leibold, M.; Kisslinger, S.; Heinemann, F.W.; Hampel, F.; Ichiyanagi, Y.; Klein, M.; Homenya, P.; Renz, F.; Toftlund, H.; Brehm, G.; *et al.* Effect of chelate ring size in iron(II) isothiocyanato complexes with tetradentate tripyridyl-alkylamine ligands on spin crossover properties. *Z. Anorg. Allg. Chem.* **2016**, *642*, 85–94. [CrossRef]
73. Wei, R.-J.; Li, B.; Tao, J.; Huang, R.-B.; Zheng, L.-S.; Zheng, Z. Making spin-crossover crystals by successive polymorphic transformations. *Inorg. Chem.* **2011**, *50*, 1170–1172. [CrossRef] [PubMed]
74. Li, B.; Wei, R.-J.; Tao, J.; Huang, R.-B.; Zheng, L.-S. Pressure effects on a spin-crossover monomeric compound [Fe(pmea)$(SCN)_2$] (pmea = bis[(2-pyridyl)methyl]-2-(2-pyridyl)ethylamine). *Inorg. Chem.* **2010**, *49*, 745–751. [CrossRef] [PubMed]
75. Nihei, M.; Shiga, T.; Maeda, Y.; Oshio, H. Spin crossover iron(III) complexes. *Coord. Chem. Rev.* **2007**, *251*, 2606–2621. [CrossRef]
76. Harding, D.J.; Harding, P.; Phonsri, W. Spin crossover iron(III) complexes. *Coord. Chem. Rev.* **2016**, *313*, 38–61. [CrossRef]
77. Watkins, D.D.; Riley, D.P.; Stone, J.A.; Busch, D.H. Iron(II) complexes with unsubstituted saturated tetraaza macrocyclic ligands of varying ring size. *Inorg. Chem.* **1976**, *15*, 387–393. [CrossRef]
78. Christiansen, L.; Hendrickson, D.N.; Toftlund, H.; Wilson, S.R.; Xie, C.-L. Synthesis and structure of metal complexes of triaza macrocycles with three pendant pyridylmethyl arms. *Inorg. Chem.* **1986**, *25*, 2813–2818. [CrossRef]
79. Al-Obaidi, A.H.R.; McGarvey, J.J.; Taylor, K.P.; Bell, S.E.J.; Jensen, K.B.; Toftlund, H. Observation of biphasic kinetics in light-induced spin-state crossover in an iron(II) complex in solution. *J. Chem. Soc. Chem. Commun.* **1993**, 536–538. [CrossRef]
80. Janiak, C.; Scharmann, T.G.; Bräuniger, T.; Holubová, J.; Nádvorník, M. Spin crossover studies on bis{hydro-tris(1,2,4-triazolyl)borato}iron(II). *Z. Anorg. Allg. Chem.* **1998**, *624*, 769–774. [CrossRef]
81. Catalan, J.; Abboud, J.L.M.; Elguero, J. Basicity and acidity of azoles. *Adv. Heterocycl. Chem.* **1987**, *41*, 187–274.
82. Sugiyarto, K.H.; Craig, D.C.; Rae, A.D.; Goodwin, H.A. Structural, magnetic and Mössbauer spectral studies of salts of bis[2,6-bis(pyrazol-3-yl) pyridine] iron(II)—A spin crossover system. *Aust. J. Chem.* **1994**, *47*, 869–890. [CrossRef]
83. Sugiyarto, K.H.; Craig, D.C.; Rae, A.D.; Goodwin, H.A. Structural and electronic properties of iron(II) and nickel(II) complexes of 2,6-bis(triazol-3-yl)pyridines. *Aust. J. Chem.* **1993**, *46*, 1269–1290. [CrossRef]
84. Baker, A.T.; Goodwin, H.A. Iron(II) and nickel(II) complexes of 2,6-di(thiazol-4-yl)pyridine and related ligands: Magnetic, spectral and structural studies. *Aust. J. Chem.* **1986**, *39*, 209–220. [CrossRef]
85. Mohammed, R.; Chastanet, G.; Tuna, F.; Malkin, T.L.; Barrett, S.A.; Kilner, C.A.; Létard, J.-F.; Halcrow, M.A. Synthesis of 2,6-di(pyrazol-1-yl)pyrazine derivatives and the spin-state behavior of their iron(II) complexes. *Eur. J. Inorg. Chem.* **2013**, *2013*, 819–831. [CrossRef]
86. Childs, B.J.; Craig, D.C.; Ross, K.A.; Scudder, M.L.; Goodwin, H.A. Structural and electronic properties of bis[2-(pyrazin-2-ylamino)-4-(pyridin-2-yl)thiazolato]iron(II) and its solvated derivatives. *Aust. J. Chem.* **1994**, *47*, 891–902. [CrossRef]
87. Tweedle, M.F.; Wilson, L.J. Variable spin iron(III) chelates with hexadentate ligands derived from triethylenetetramine and various salicylaldehydes. Synthesis, characterization, and solution state studies of a new $^2T \rightleftharpoons {}^6A$ spin equilibrium system. *J. Am. Chem. Soc.* **1976**, *98*, 4824–4834. [CrossRef]
88. Masárová, P.; Zoufalý, P.; Moncol, J.; Nemec, I.; Pavlik, J.; Gembický, M.; Trávníček, Z.; Boča, R.; Šalitroš, I. Spin crossover and high spin electroneutral mononuclear iron(III) Schiff base complexes involving terminal pseudohalido ligands. *New J. Chem.* **2015**, *39*, 508–519. [CrossRef]
89. Hansch, C.; Leo, A.; Taft, R.W. A survey of Hammett substituent constants and resonance and field parameters. *Chem. Rev.* **1991**, *91*, 165–195. [CrossRef]
90. Nakano, K.; Suemura, N.; Yoneda, K.; Kawata, S.; Kaizaki, S. Substituent effect of the coordinated pyridine in a series of pyrazolato bridged dinuclear diiron(II) complexes on the spin-crossover behavior. *Dalton Trans.* **2005**, 740–743. [CrossRef] [PubMed]
91. Létard, J.-F.; Carbonera, C.; Real, J.A.; Kawata, S.; Kaizaki, S. Photomagnetism of a series of dinuclear iron(II) complexes. *Chem. Eur. J.* **2009**, *15*, 4146–4155. [CrossRef] [PubMed]

92. Houghton, J.; Deeth, R.J. Spin-state energetics of Fe^{II} complexes—The continuing voyage through the density functional minefield. *Eur. J. Inorg. Chem.* **2014**, 4573–4580. [CrossRef]
93. Takahashi, K.; Hasegawa, Y.; Sakamoto, R.; Nishikawa, M.; Kume, S.; Nishibori, E.; Nishihara, H. Solid-state ligand-driven light-induced spin change at ambient temperatures in bis(dipyrazolylstyryl-pyridine)iron(II) complexes. *Inorg. Chem.* **2012**, *51*, 5188–5198. [CrossRef] [PubMed]
94. Creutz, S.E.; Peters, J.C. Spin-state tuning at pseudo-tetrahedral d^6 ions: Spin crossover in $[BP_3]Fe^{II}-X$ complexes. *Inorg. Chem.* **2016**, *55*, 3894–3906. [CrossRef] [PubMed]
95. Park, J.G.; Jeon, I.-R.; Harris, T.D. Electronic effects of ligand substitution on spin crossover in a series of diiminoquinonoid-bridged Fe^{II}_2 complexes. *Inorg. Chem.* **2015**, *54*, 359–369. [CrossRef] [PubMed]
96. Enamullah, M.; Hasegawa, M.; Fukuda, Y.; Linert, W.; Hoshi, T. Synthesis, characterization and spin-crossover behaviors of [Co(hydroxycarboxylato)(triphos)] complexes. *Bull. Chem. Soc. Jpn.* **2002**, *75*, 2449–2453. [CrossRef]
97. Kershaw Cook, L.J.; Kulmaczewski, R.; Mohammed, R.; Dudley, S.; Barrett, S.A.; Little, M.A.; Deeth, R.J.; Halcrow, M.A. A unified treatment of the relationship between ligand substituents and spin state in a family of iron(II) complexes. *Angew. Chem. Int. Ed.* **2016**, *55*, 4327–4331. [CrossRef] [PubMed]
98. Roberts, T.D.; Little, M.A.; Kershaw Cook, L.J.; Halcrow, M.A. Iron(II) complexes of 2,6-di(1*H*-pyrazol-3-yl)pyridine derivatives with hydrogen bonding and sterically bulky substituents. *Dalton Trans.* **2014**, *43*, 7577–7588. [CrossRef] [PubMed]
99. Turner, J.W.; Schultz, F.A. Solution characterization of the iron(II) bis(1,4,7-triazacyclononane) spin-equilibrium reaction. *Inorg. Chem.* **2001**, *40*, 5296–5298. [CrossRef] [PubMed]
100. Chum, H.L.; Vanin, J.A.; Holanda, M.I.D. Tris(2-(aminomethyl)pyridine)iron(II): A new spin-state equilibrium in solution. *Inorg. Chem.* **1982**, *21*, 1146–1152. [CrossRef]
101. Linert, W.; Konecny, M.; Renz, F. Spin-state equilibria in non-aqueous solution and quantum mechanical investigations of iron(II) and nickel(II) complexes with 4-substituted 2,6-bis(benzimidazol-2-yl)pyridines. *J. Chem. Soc. Dalton Trans.* **1994**, 1523–1531. [CrossRef]
102. Ni, Z.; Shores, M.P. Magnetic observation of anion binding in iron coordination complexes: Toward spin-switching chemosensors. *J. Am. Chem. Soc.* **2009**, *131*, 32–33. [CrossRef] [PubMed]
103. Ni, Z.; McDaniel, A.M.; Shores, M.P. Ambient temperature anion-dependent spin state switching observed in "mostly low spin" heteroleptic iron(II) diimine complexes. *Chem. Sci.* **2010**, *1*, 615–621. [CrossRef]
104. Ni, Z.; Shores, M.P. Supramolecular effects on anion-dependent spin-state switching properties in heteroleptic iron(II) complexes. *Inorg. Chem.* **2010**, *49*, 10727–10735. [CrossRef] [PubMed]
105. Ni, Z.; Fiedler, S.R.; Shores, M.P. Investigation of anion-dependence in the spin-state switching properties of $[(H_2bip)_2Fe(6\text{-Mebpy})]X_2$. *Dalton Trans.* **2011**, *40*, 944–950. [CrossRef] [PubMed]
106. Barrett, S.A.; Halcrow, M.A. Anion-dependent spin crossover in solution for an iron(II) complex of a 1*H*-pyrazolyl ligand. *RSC Adv.* **2014**, *4*, 11240–11243. [CrossRef]
107. Kubik, S. Anion recognition in water. *Chem. Soc. Rev.* **2010**, *39*, 3648–3663. [CrossRef] [PubMed]
108. Young, M.C.; Liew, E.; Ashby, J.; McCoy, K.E.; Hooley, R.J. Spin state modulation of iron spin crossover complexes via hydrogen-bonding self-assembly. *Chem. Commun.* **2013**, *49*, 6331–6333. [CrossRef] [PubMed]
109. Young, M.C.; Liew, E.; Hooley, R.J. Colorimetric barbiturate sensing with hybrid spin crossover assemblies. *Chem. Commun.* **2014**, *50*, 5043–5045. [CrossRef] [PubMed]
110. Barbour, L.J. X-seed—A software tool for supramolecular crystallography. *J. Supramol. Chem.* **2001**, *1*, 189–191. [CrossRef]
111. Groom, C.R.; Bruno, I.J.; Lightfoot, M.P.; Ward, S.C. The Cambridge structural database. *Acta Cryst. Sect. B Struct. Sci. Cryst. Eng. Mater.* **2016**, *72*, 171–179. [CrossRef] [PubMed]
112. *SIGMAPLOT*; v. 8.02; SPSS Scientific Inc.: Chicago, IL, USA, 2002.